Characterization of fiber-generated entangled photon pairs with superconducting single-photon detectors

Chuang Liang, Kim Fook Lee, Milja Medic, and Prem Kumar

Center for Photonic Communication and Computing,
Department of Electrical Engineering and Computer Science,
Northwestern University, 2145 Sheridan Road, Evanston, IL 60208-3118
liang@ece.northwestern.edu

Robert H. Hadfield and Sae Woo Nam

National Institute of Standards and Technology, 325 Broadway, Boulder, Colorado 80305

Abstract: We demonstrate the suitability of fiber-generated entangled photon pairs for practical quantum communications in the telecom band by measuring their properties with superconducting single-photon detectors that produce negligible dark counts. The photon pairs are created in approximately 5-ps duration windows at 50 MHz rate while the detectors are operated in ungated free running mode. We obtain a coincidence to accidental-coincidence ratio >80 with raw photon-counting data, i.e., without making any post-measurement corrections. Using a previously demonstrated counter-propagating scheme we also produce polarization-entangled photon pairs at 50-MHz rate, which in coincidence detection directly yield two-photon interference with a fringe visibility >98%.

OCIS codes: (270.0270) Quantum optics; (190.4370) Nonlinear optics, fibers; (999.9999) Quantum communications; (060.0060) Fiber optics and optical communications, (040.5570) Quantum detectors.

References and links

1. M. Fiorentino, P. L. Voss, J. E. Sharping, and P. Kumar, "All-fiber photon-pair source for quantum communication," Photon. Technol. Lett. **14**, 983–985 (2002).
2. X. Li, J. Chen, P. L. Voss, J. Sharping, and P. Kumar, "All-fiber photon-pair source for quantum communications: improved generation of correlated photons," Opt. Express **12**, 3737–3744 (2004).
3. J. Rarity, J. Fulconis, J. Duligall, W. Wadsworth, P. Russell, "Photonic crystal fiber source of correlated photon pairs," Opt. Express **13**, 534-544(2005).
4. X. Li, P. L. Voss, J. E. Sharping, and P. Kumar, "Optical-Fiber Source of Polarization-Entangled Photons in the 1550 nm Telecom Band," Phys. Rev. Lett. **94**, 053601 (2005).
5. H. Takesue and K. Inoue, "1.5-um band quantum-correlated photon pair generation in dispersion-shifted fiber: suppression of noise photons by cooling fiber," Opt. Express **13**, 7832 (2005).
6. X. Li, C. Liang, K. F. Lee, J. Chen, P. L. Voss, and P. Kumar, "An integrable optical-fiber source of polarization-entangled photon pairs in the telecom band," Phys. Rev. A **73**, 052301 (2006).
7. K. F. Lee, J. Chen, C. Liang, X. Li, P. L. Voss, and P. Kumar, "Generation of high-purity telecom-band entangled-photon pairs in dispersion-shifted fiber," Opt. Lett. **31**, 1905–1907 (2006).
8. B. Cabrera, R. M. Clarke, P. Colling, A. J. Miller, S. Nam, and R. W. Romani, "Detection of single infrared, optical, and ultraviolet photons using superconducting transition edge sensors," Appl. Phys. Lett. **73**, 735 (1998).
9. G. Gol'tsman, O. Okunev, G. Chulkova, A. Lipatov, A. Semenov, K. Smirnov, C. Williams, and R. Sobolewski, "Picosecond superconducting single-photon optical detector," Appl. Phys. Lett. **79**, 705 (2001).
10. B. S. Robinson, A. J. Kerman, E. A. Dauler, R. J. Barron, D. O. Caplan, M. L. Stevens, J. J. Carney, S. A. Hamilton, J. K. W. Yang, and K. K. Berggren, "781 Mbit/s photon-counting optical communications using a superconducting nanowire detector," Opt. Lett. **31**, 444 (2006).

#77220 - $15.00 USD Received 21 November 2006; revised 15 January 2007; accepted 18 January 2007

11. M. A. Jaspan, J. L. Habif, R. H. Hadfield, and S. W. Nam, "Heralding of telecommunication photon pairs with a superconducting single photon detector," Appl. Phys. Lett. **89**, 031112 (2006).
12. R. H. Hadfield, M. J. Stevens, S. S. Gruber, A. J. Miller, R. E. Schwall, R. P. Mirin, and S. W. Nam, "Single photon source characterization with a superconducting single photon detector," Opt. Express **13**, 10846 (2005).

Since the first report on the generation of quantum-correlated photon pairs in the telecom band with use of optical fiber's Kerr nonlinearity [1-3], significant progress has been made in improving the fidelity of the generated entanglement [4-6]. The fidelity can be measured by employing two metrics: i) the ratio of measured coincidence counts to accidental coincidence counts, conveniently referred to as CAR; and ii) the measured visibility of the fringe obtained via two-photon interference (TPI). By cooling the fiber to liquid nitrogen temperature, a CAR of greater than 100 has been achieved and a TPI visibility of over 98% has been obtained [7]. However, in all the measurements reported to date, the data are usually corrected by subtracting the contribution from dark counts produced in the detectors. The correction is necessary because the single-photon detectors that are generally used to measure the 1550 nm telecom-band photons have a significantly high dark-count probability during the detection time owing to the high dark current of InGaAs avalanche photodiodes (APDs) employed in such detectors. Therefore, the suitability of the fiber-nonlinearity based entanglement sources in practical quantum information processing has remained an open question, since the results of raw measurements must be used in any realistic quantum information protocol. In this paper we provide an affirmative answer to the suitability question by presenting measurements of the CAR and TPI visibility that are made with a superconducting single-photon detector (SSPD) having a negligible dark-count rate.

In recent years, superconducting devices have been developed for ultra-low-noise detection of telecom-band photons. Two classes of devices have been reported: transition edge sensors [8] offer detection efficiencies up to 90% and an ability to resolve photon number, but they require ~100 mK operating temperature and are limited at present to detection rates on the order of kilohertz. NbN-based SSPDs [9-10], on the other hand, have relatively lower detection efficiencies (≤5%) in devices demonstrated to date, but they can be operated at 4 K temperature with detection rates approaching a gigahertz. An SSPD is a meander-shaped nanoscale superconducting wire that is current biased slightly below its critical current. The energy of an absorbed photon forms a hotspot in the wire, momentarily breaking the superconductivity and causing a transient voltage in the external circuit that can be registered as a detection event. Unlike InGaAs APDs, the dark-count probability of superconducting detectors is low even without gating, making them useful devices for quantum-communication applications in the telecom band [11]. In the following, we present a full characterization of fiber-generated entanglement using SSPDs integrated into a cryogen-free system [12].

Figure 1(a) shows a schematic of the counter propagating scheme [4-6] for generating polarization-entangled photon pairs by pumping the fiber nonlinearity. A 1555.95-nm wavelength, 50-MHz repeated train of ~5-ps duration pump pulses is obtained by sending the output pulses of ~100-fs duration from a passively-mode-locked fiber laser through a cascade of 200-GHz spacing, ITU-grid aligned, wavelength division multiplexing, fiber-pigtailed filters. A polarizer regulates the incoming pump pulses to 45° linearly polarized relative to the principal axes of a polarization beam splitter (PBS). The 300-m long DSF, whose zero-dispersion wavelength is around 1556 nm, is connected to the two output ports of the PBS. Thus, the DSF is simultaneously pumped with orthogonally-polarized pump pulses in the clockwise and counter-clockwise directions. As the two counter-propagating pump-pulse trains travel through the DSF, they independently engage in four-photon-scattering processes and create quantum-correlated photon pairs. The counter-propagating photon pairs and their parent pump pulses recombine upon arrival back at the PBS and emerge from the opposite

#77220 - $15.00 USD Received 21 November 2006; revised 15 January 2007; accepted 18 January 2007

input port. Another cascade of 200-GHz-spacing filters, which are widely deployed in high-speed optical communication systems as wavelength division multiplexers (WDMs), is used to separate the newly born photon pairs from the pump pulses. Each WDM filter set provides ≥70 dB isolation in the signal and idler bands from the pump. The WDM filters have a passband shape that fits very well to a fourth-order super-Gaussian function with a full width at half maximum of 1 nm [6]. At low pump powers, the generated signal-idler photon pairs of 1550.92-nm and 1561.01-nm wavelengths, respectively, are in a maximally-entangled state: $|H\rangle_s|H\rangle_i+|V\rangle_s|V\rangle_i$. The system can also be configured as a correlated photon-pair source when the linear polarizer is oriented parallel to one principal axis of the PBS [see Fig. 1(a)] so that the DSF is pumped only in one direction. The DSF is cooled to liquid nitrogen temperature for suppressing the Raman-scattered photons.

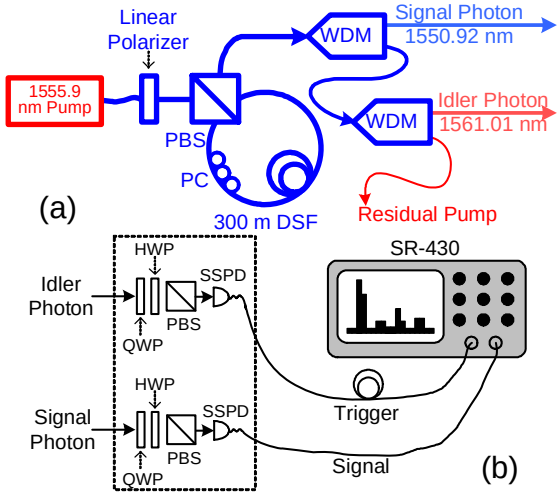

FIG. 1. Schematic of the experimental setup: (a) Optical-fiber source of polarization-entangled photon pairs with use of a counter propagating scheme. (b) Polarization entanglement analyzer. HWP, half-wave plate; QWP, quarter-wave plate; DSF, dispersion-shifted fiber; WDM, wavelength division multiplexers, which are employed as pump-rejection filters; PBS, polarization beam splitter; PC, polarization controller; SR-430, multichannel scaler/averager.

Figure 1(b) depicts the measurement apparatus for detecting and evaluating the photon pairs. Signal and idler photons are sent to different polarization analyzers. Each analyzer set contains a QWP-HWP polarization rotator, a PBS, and a SSPD operated at ~2.9 K temperature. Detection signals from the SSPDs are fed to a photon counter (Stanford Research Systems, model SR-400) which serves as a counts monitor and discriminator. Each time a detection event is registered by the SR-400 it generates a pulse of 10 ns duration. A multi-channel scaler/averager (Stanford Research Systems, model SR-430) is employed for determining the correlations between the signal-photon and the idler-photon detection events. As shown in Fig. 1(b), an idler-photon detection event from the SR-400 triggers the SR-430, which then segments the arrival of signal-photon detection events into sequential 1024 time bins. The width of each bin is set to 5 ns. The instrument records the number of counts that arrive in each time bin after the trigger. After accumulating data for multiple trigger trials, the SR-430 generates a histogram that is proportional to the temporal correlation function between the signal-photon and the idler-photon detection events. The number of coincidence counts and the accidental-coincidence counts, and hence the CAR, can be determined from this histogram.

At low photon production rates, the probabilities of detection events are given by $\eta_s(\mu+\mu_b)+p_d^s$ and $\eta_i(\mu+\mu_b)+p_d^i$ for the signal and idler time windows, respectively. The probabilities of true coincidences and accidental coincidences can be written as $C=\eta_s\eta_i\mu$

#77220 - $15.00 USD Received 21 November 2006; revised 15 January 2007; accepted 18 January 2007

and $A = \eta_s \eta_i (\mu + \mu_b)^2 + \eta_s (\mu + \mu_b) p_d^i + \eta_i (\mu + \mu_b) p_d^s + p_d^s p_d^i$, respectively; where μ is the probability of an entangled-pair being produced in the measured time window; μ_b is the probability of a background photon in each time window, which occurs predominately due to Raman scattering of the pump pulses; p_d^s (p_d^i) is the probability of a dark count from the signal (idler) SSPD in the measured time window; η_s (η_i) is the total detection efficiency for the signal (idler) photons, including the SSPD quantum efficiency and the 5.4 dB optical loss from the pair-production site in the DSF to the detector. Under the experimental conditions: $(\mu + \mu_b) \sim 0.01$, p_d^s and $p_d^i \sim 10^{-6}$, the expected CAR can be approximately written as:

$$\text{CAR} \cong \eta_s \eta_i \mu / [\eta_s \eta_i (\mu + \mu_b)^2 + \eta_s (\mu + \mu_b) p_d^i + \eta_i (\mu + \mu_b) p_d^s] \quad (1)$$

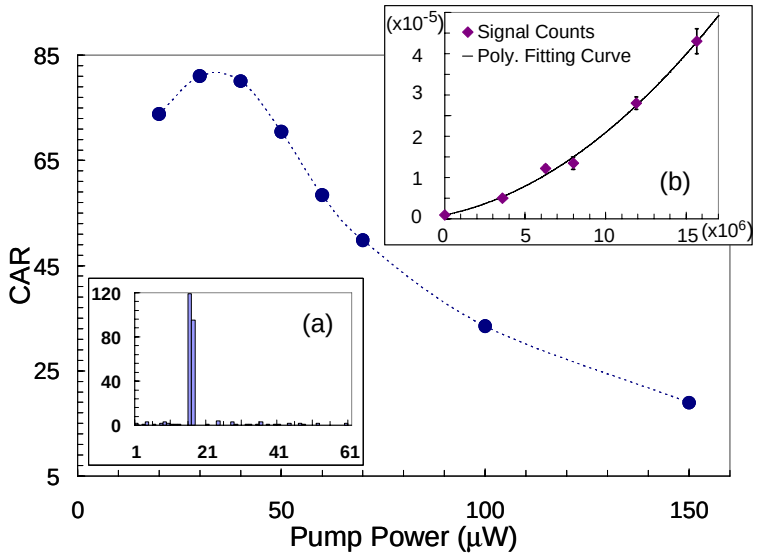

FIG. 2. Variation of the coincidence to accidentals ratio (CAR) versus average pump power (solid circles). The dashed curve is to guide the eye only. Inset (a) is a sample histogram (abscissa: time-bin number; ordinate: counts in 400,048 trials) from the SR430 for a pump power of 30 μW. Inset (b) shows the detected signal counts (solid diamonds) versus the pump power (abscissa: number of pump photons per pulse; ordinate: number of counts per pump pulse). A second-order-polynomial fit (solid curve) to the experimental data is also shown.

Figure 2 shows our CAR measurement results. During these measurements, we set the bias currents to be such that the dark-count rate from the signal (idler) SSPD is ≅40/s (≅60/s). Inset (a) in Fig. 2 is a sample histogram recorded by the SR-430 at a pump power of 30 μW after accumulating 400,048 trigger trials. Two time bins in the histogram should be counted as one since the discriminator pulses from the SR-400 are of 10 ns duration whereas each time bin of the SR-430 is set to 5 ns. The main peak in the histogram appears in time bins 16 and 17 and corresponds to coincidence counts where the time delay between signal-photon detection events and idler-photon detection events is zero. Other time bins in the histogram represent the cases of accidental coincidences. The number of coincidence counts is directly obtained by adding the number of counts in the two time bins of the main peak. The data in the remaining time bins are used to compute the number of accidental-coincidence counts by taking the average number of counts per four time bins, which corresponds to the 20 ns interval between 50-MHz repeated pump pulses. The resulting CAR is then plotted versus pump power in the main body of Fig. 2. A CAR of 81 is observed for average pump powers between 30 to 40 μW without making any post-measurement correction. [Note that the actual CAR is possibly higher since the above method slightly overestimates the accidental

#77220 - $15.00 USD Received 21 November 2006; revised 15 January 2007; accepted 18 January 2007

coincidences. This is because the dark counts from the SSPDs (e.g., the counts in bins 12 and 13 of the inset (a) in Fig. 2), which are asynchronous with the pump pulses, could potentially be discriminated by gating the SSPD outputs.] The CAR decreases as the pump power is increased beyond the approximately 35-μW optimum value. This is due to the additional accidental coincidences resulting from the first term in the denominator of Eq. (1). At pump powers below 20 μW, the low photon-pair generation rate leads to a decreasing CAR due to insufficient signal-to-noise ratio in the measured quantities.

Inset (b) of Fig. 2 plots the number of detected counts per pulse, N_s, in the signal channel versus the number of pump photons, N_p, per pulse. A 2nd-order polynomial $N_s = N_0 + s_1 N_p + s_2 N_p^2$ (solid curve) is shown to fit the data very well, wherein N_0 is the contribution from the SSPD dark counts, $s_1 N_p$ is that from Raman scattered photons, and $s_2 N_p^2$ is that from the pair-wise generation of signal-idler photons. s_1 and s_2 are linear and quadratic fitting coefficients proportional to the total detection efficiency and are related to the Raman photon and correlated photon-pair generation rates, respectively. A detailed analysis can be found in Ref. 2. The fitting parameters used to plot the dashed curve in inset (b) of Fig. 2 give: $N_0 \cong 8 \pm 2 \times 10^{-7}$, $s_1 \cong 8 \pm 2 \times 10^{-13}$, and $s_2 \cong 1.2 \pm 0.2 \times 10^{-19}$. At 40 μW average pump power, we estimate a CAR of $\cong 88$ using Eq. (1) and the measured $\eta_s \cong 2.3 \times 10^{-3}$, $\eta_i \cong 2.1 \times 10^{-3}$, $\mu \cong 2.2 \times 10^{-3}$, $(\mu + \mu_b) \cong 4.6 \times 10^{-3}$, $p_d^s \cong 6 \times 10^{-7}$, and $p_d^i \cong 1.2 \times 10^{-6}$. The measured CAR of 81 matches the estimated value very well.

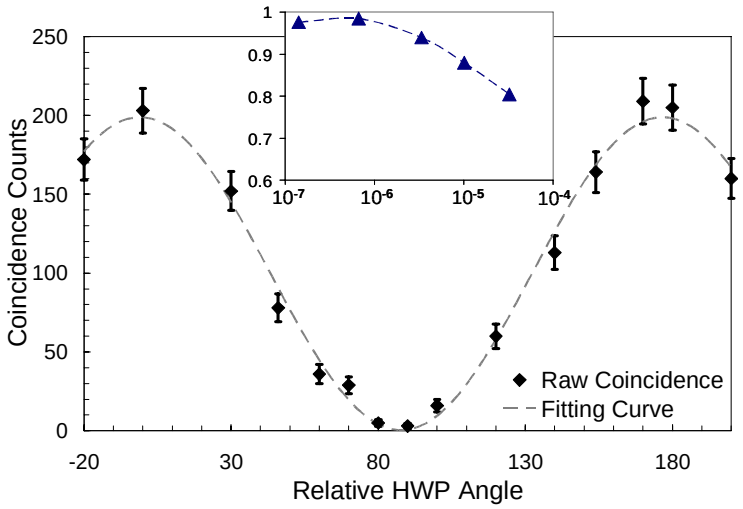

FIG. 3. Results of two-photon-interference (TPI) measurements. The inset shows crudely measured TPI fringe visibility versus SSPD dark-count probability during 20 ns.

Next, we configure the source to emit polarization-entangled photon pairs. We use 40 μW of average pump power, which is in the optimum range (see Fig. 2) and produces $\cong 4.4 \times 10^{-3}$ entangled pairs/pulse. The DSF is pumped with two counter-propagating orthogonally-polarized pumps of 40 μW average power each. Since all created photon pairs are collected in the CPS scheme [6], the total production rate doubles. Thus the source emits 2.2×10^5 entangled photon pairs/s at 50 MHz pump rate. In order to configure the SSPDs for an optimum combination of detection efficiencies and dark-count-probabilities, we first crudely obtain the TPI fringe visibility for various detector bias currents by recording the coincidence counts at analyzer settings corresponding to the peak C_{max} and valley C_{min} of the TPI fringe.

#77220 - $15.00 USD Received 21 November 2006; revised 15 January 2007; accepted 18 January 2007

TPI visibility is then estimated as $(C_{\max} - C_{\min})/(C_{\max} + C_{\min})$. The results are plotted in the inset of Fig. 3, where the abscissa is the geometric mean $p_d^a = (p_d^s p_d^i)^{1/2}$ evaluated over 20 ns. It shows that a TPI visibility of ~98% can be achieved for $p_d^s < 10^{-6}$ counts per 20 ns. Hence we set the SSPD bias currents such that they yield similar detection efficiencies with a dark count of ≅40/s (≅70/s) for the signal (idler) SSPD corresponding to a quantum efficiency of ~0.46% (~0.50%). Then we measure the TPI fringe by recording the coincidence counts (total of counts in the two coincident bins of the SR-430 histograms) as a function of the relative angle θ between the orientations of the HWPs in the two analyzers. As shown in Fig. 3, the $|H\rangle_s|H\rangle_i+|V\rangle_s|V\rangle_i$ polarization entanglement gives rise to a TPI fringe on the coincidence counts in the form of $\cos^2\theta$, while almost constant numbers of counts are observed for all angle settings from individual measurements of either the signal (≅550 counts/s) or idler (≅600 counts/s) photons. Each data point is obtained after integrating over 400,048 trigger trials. The $\cos^2\theta$ fitting curve (dashed) suggests a TPI fringe visibility >98%. No post-measurement correction is employed (neither the dark counts nor the accidental coincidences are subtracted) in obtaining these results.

The >80 CAR and over 98% TPI visibility from direct measurement with SSPDs assure the high quality of the telecom-band entangled photon pairs produced by the fiber-nonlinearity based source. It is also important to point out that these measurements are performed in a free-running mode as opposed to the previously reported gated-operation mode. We have measured the 50-MHz pumped entangled-photon source at its full rate. It is the low detection efficiency of the SSPDs that gives rise to a considerably lower detected coincidence rate. These results, which employ no post-measurement corrections, confirm our previous conclusion in Refs. 1–7 that high-fidelity entanglement in the telecom band can be obtained with fiber-nonlinearity based photon-pair generation. Together with other features of the fiber sources, such as negligible coupling loss to the transmission fiber and high spatial-mode purity, we conclude that such entanglement sources are ripe for implementing practical quantum communication applications such as quantum cryptography and distributed quantum information processing.

Acknowledgments

This work is supported in part by the NSF under grant EMT-0523975 and by DARPA under grant F30602-01-2-0528. RHH and SWN acknowledge support from the NIST QI program and thank A. J. Miller and R. E. Schwall for technical assistance. We thank G. Gol'tsman (Moscow) for providing the basic detectors used in this experiment. The use of a trade name does not imply endorsement by NIST.

#77220 - $15.00 USD Received 21 November 2006; revised 15 January 2007; accepted 18 January 2007